Copy 6
RM L52L11

RESEARCH MEMORANDUM

EXPERIMENTAL INVESTIGATION OF THE FLOW FIELD BEHIND AN ASPECT-RATIO-10 HYDROFOIL NEAR THE WATER SURFACE

By Arthur W. Carter and Roger V. Butler

Langley Aeronautical Laboratory
Langley Field, Va.

NATIONAL ADVISORY COMMITTEE
FOR AERONAUTICS

WASHINGTON

February 24, 1953

NACA RM L52L11

NATIONAL ADVISORY COMMITTEE FOR AERONAUTICS

RESEARCH MEMORANDUM

EXPERIMENTAL INVESTIGATION OF THE FLOW FIELD BEHIND AN ASPECT-RATIO-10 HYDROFOIL NEAR THE WATER SURFACE

By Arthur W. Carter and Roger V. Butler

SUMMARY

An investigation was made at subcritical speeds in Langley tank no. 1, of the flow field behind a hydrofoil having an 8-inch chord and an aspect ratio of 10, and operating at a depth of 0.75 chord below the free-water surface. The downwash and water surface profiles were measured behind the hydrofoil over a range of lateral and longitudinal positions of interest for tandem hydrofoil applications. The experimental data were compared with theoretical predictions based on two-dimensional flow.

As predicted by theory, the displacement of the free-water surface and the angles of downwash varied directly with lift coefficient. The angles of downwash varied exponentially with depth below the water surface as would be expected for gravity waves. In the region investigated, the surface wave can be predicted by two-dimensional theory from the trailing edge to the point of maximum upwash, but only at low subcritical speeds and near the center line. The angles of downwash can be predicted by two-dimensional theory over the same range for which the theory accurately predicts the surface wave. Outboard of the center plane, the surface and downwash patterns were complicated by the tip disturbances and no valid comparison with two-dimensional theory was possible.

INTRODUCTION

As part of the general research on hydrofoils, an investigation has been made of the flow field behind a high-aspect-ratio rectangular hydrofoil operating near the water surface. The purpose of the investigation was to determine the downwash pattern behind the hydrofoil and to determine the regions over which predictions, using available theory, were accurate. Theoretical methods for calculating the length and amplitude of the surface wave behind the hydrofoil and the angles of downwash below the free-water surface in two-dimensional flow have been presented in references 1 and 2.

The downwash and water-surface profiles behind a hydrofoil having an NACA 64_1A412 section and aspect ratio of 10 were determined in Langley tank no. 1, over a range of lateral and longitudinal positions of interest in tandem hydrofoil applications. This information is of interest in predicting the effects of the front hydrofoil on the characteristics of the second hydrofoil and in determining the over-all lift and drag as well as the stability and control of the system.

SYMBOLS

C_L	hydrofoil lift coefficient
c_l	local lift coefficient
a	distance from plane of symmetry, ft
b	semispan of hydrofoil, ft
c	chord of hydrofoil, ft
d	depth below free-water surface, ft
f	depth of hydrofoil submergence, ft
g	acceleration due to gravity (32.2), ft/sec^2
h	mean depth of tank (10.6), ft
l	distance aft of trailing edge of hydrofoil, ft
V	speed, fps
x	distance aft of quarter chord of hydrofoil, ft
y	displacement of free-water surface, positive upward, chords
y_o	displacement of free-water surface, positive upward, ft
α	angle of attack, deg
Γ	circulation, ft^2/sec
ϵ	angle of downwash, deg
λ	wave length, ft

[redacted]

PRELIMINARY CONSIDERATIONS

In line with usual theories of wave motion, two distinctly different wave patterns exist in shallow water: one if the velocity is subcritical, the other if the velocity is supercritical. (See ref. 1.) The critical velocity depends upon the depth of the channel and is defined by $\sqrt{gh}$. In Langley tank no. 1, the critical velocity is 18.5 feet per second for the mean depth of 10.6 feet.

At subcritical speeds, the bound vortex of a hydrofoil operating near the water surface produces a deformation of the free surface in such a manner that a train of transverse surface waves is generated which has a forward speed equal to the speed of the hydrofoil. At supercritical speeds, the transverse waves disappear. At subcritical speeds, the downwash field behind the hydrofoil will be modified by the pressure field set up by the surface waves. According to reference 3, the effect of the depth of water on the wave formation becomes appreciable for values of V^2/gh greater than 0.5. The present investigation was made at two values below 0.5 and one above.

DESCRIPTION OF MODEL, APPARATUS, AND PROCEDURE

The hydrofoil (fig. 1) had an NACA 64_1A412 section, an 8-inch chord, and an aspect ratio of 10. The hydrofoil was supported by a single strut which had an NACA 66_1-012 section and an 8-inch chord. The intersection of the hydrofoil and strut was not filleted. A detailed description of the hydrofoil and strut and the section ordinates are given in reference 4.

The hydrofoil and the supporting gear, which were the same as those used for the investigation described in reference 4, were mounted on an auxiliary carriage ahead of the main towing carriage in Langley tank no. 1. Two 20-foot booms connecting the auxiliary carriage to the main carriage served as a support for the survey gear (fig. 2) used to determine the flow field. The survey gear could be moved longitudinally and laterally in order to survey any desired position in the flow field of the hydrofoil.

The direction of the flow was determined from photographs of tufts attached to the survey gear. Four horizontal wires between two vertical $1\frac{1}{2}$-inch streamline struts, 12 inches apart, served as attachment points for the tufts. The wires were located 6, 12, 18, and 24 inches below the undisturbed water surface. Of several types of wires investigated, $\frac{1}{32}$-inch aircraft cable appeared to be the most suitable inasmuch as this wire was relatively free from vibration. The tufts were 5-inch-long threads of

[redacted]

Fiberglas attached to the center of the cable so that they were free to turn about the cable. Fiberglas was used because it was flexible, durable, and easily photographed. Wool, nylon, cotton, and linen tufts disintegrated after relatively few runs.

The tufts were photographed from the side of the tank by a camera whose lens was 1 foot below the water surface. A typical underwater photograph is shown in figure 3. The vertical line is a reference plumb bob line in the tank. Angles of downwash were measured relative to this reference.

The displacement of the free-water surface was measured by means of the surface prod shown in figure 2. The prod was lowered slowly until contact was made with the water surface, thereby closing an electrical circuit which tripped a camera and photographed a scale. A water-level recorder was located at each of the two test stations in the tank so that small changes in the reference level caused by the surge in the tank could be made. The correction to the surface data because of the surge was generally less than 0.1 inch.

The flow field was investigated at the following test conditions:

(a) Angles of attack: 2°, 4°, and 6°

(b) Constant speeds: 8.3, 11.7, and 14.3 feet per second, corresponding to values of V^2/gh of 0.2, 0.4, and 0.6

(c) Lateral positions: 0.1, 0.5, 0.9, and 1.3 semispan from plane of symmetry

(d) Longitudinal positions: leading edge to 3$\frac{8}{}$ chords behind trailing edge of hydrofoil

The measurements are believed to have the following accuracy:

Angle of downwash, deg	±0.2
Displacement of free-water surface, in.	±0.2

RESULTS AND DISCUSSION

The complex shape of the water surface behind an aspect-ratio-10 hydrofoil is shown in figure 4, which is a photograph of a model of a typical water-surface pattern. This surface pattern was developed from the surface measurements made at the four spanwise positions and is symmetrical about the center line. The vertical scale of the model is increased five times in order to show more clearly the shape of the

surface. The transverse lines are at 2-chord intervals from the hydrofoil trailing edge which is indicated on the model.

The surface behind the hydrofoil was not a simple transverse wave. The typical surface pattern shown in figure 4 was obtained at a speed corresponding to V^2/gh of 0.4 and an angle of attack of 4°. Disturbances, originating near the tips of the hydrofoil, traveled inward and intersected on the center line about 20 chords behind the trailing edge. Immediately behind the peak or crest formed by the intersection of the disturbances, a sharp depression was formed. Thus, even at the center line, the influence of the disturbances from the tips became evident at a relatively short distance behind the trailing edge of the hydrofoil. The tip disturbance, therefore, has a pronounced effect on the wave following the hydrofoil. The supporting strut created a small disturbance at the center, near the trailing edge. At 0.1 semispan, the strut disturbance was negligible at the low speeds used in the investigation.

Surface Contours

Longitudinal variation.- Longitudinal surface profiles behind the hydrofoil at the 0.1 semispan position are presented in figure 5 for values of V^2/gh of 0.2, 0.4, and 0.6. The displacement of the free-water surface in chords divided by the local lift coefficient at 0.1 semispan has been plotted against distance behind the trailing edge in chords. The local lift coefficient was used because this lift coefficient is significant for a particular semispan position. The local lift coefficients were determined from the spanwise loading by the method presented in reference 5. The hydrofoil lift coefficients used in determining the local lift coefficients were obtained from previous force measurements on the hydrofoil as reported in reference 6. The hydrofoil lift coefficients and the local lift coefficients are presented in table I. When the displacement of the water surface for angles of attack of 2°, 4°, and 6° were divided by the local lift coefficient, the data collapsed and the displacement of the free-water surface behind the hydrofoil, therefore, varied directly with lift coefficient.

A single curve was faired through the data at each value of V^2/gh. A sine wave was fitted to the data from the trough behind the hydrofoil to the free-water surface or from the point of zero upwash to the point of maximum upwash for the first wave. The sine curve was started at a point on the free-water surface directly above the quarter chord of the hydrofoil and was extended to a point just beyond the crest of the following wave.

At the first crest behind the hydrofoil, the observed amplitude was greater than that of the fitted sine wave at V^2/gh of 0.2, but less at

higher speeds. The surface disturbances originating near the tips of the hydrofoil appeared to have an appreciable influence on the amplitude of the displacement of the water surface near the crest of the following wave.

Spanwise variation.- Longitudinal surface profiles behind the hydrofoil at a 4° angle of attack for four spanwise positions are presented in figures 6(a), 6(b), and 6(c) for values of V^2/gh of 0.2, 0.4, and 0.6, respectively. In general, the profiles approximated a sine function for the first half-length except at the 0.5-semispan position. The inflection in the profiles at 0.5 semispan was caused by the disturbance from the tip of the hydrofoil. (See fig. 4.)

As shown in figure 6, the maximum displacement of the water surface in the trough decreased and moved aft as the distance from the center plane was increased. The decrease in amplitude apparently was associated with the decrease in local lift coefficients as the tips of the hydrofoil were approached.

In general, the water just behind the trailing edge of the hydrofoil was displaced downward, except outboard of the tip of the hydrofoil where the water surface was displaced upward. The distance aft of the hydrofoil over which the water was displaced upward and the magnitude of this displacement increased with increase in value of V^2/gh. This behavior would be expected because the strength of the trailing vortices increases with increase in speed for a constant angle of attack.

Comparison of Surface Profiles With Theoretical Two-Dimensional Waves

The equation for displacement of the free-water surface for two-dimensional subcritical flow has been developed by Meyer and is presented in reference 2. The equation is as follows:

$$y_o = \frac{\Gamma}{V}\left\{\frac{2 \sinh\left[\left(1 - \frac{f}{h}\right)u_o\right]\cosh(u_o)}{\frac{gh}{V^2} - \cosh^2(u_o)}\right\}\sin\left(\frac{x}{h}u_o\right) +$$

$$\frac{\Gamma}{V}\left\{\sum_{n=1}^{\infty}\frac{\sin\left[\left(1 - \frac{f}{h}\right)v_n\right]\cos(v_n)e^{-\frac{|x|}{h}v_n}}{\frac{gh}{V^2} - \cos^2(v_n)}\right\}$$

[redacted]L

In the equation on the preceding page $|x|$ indicates the absolute value of x. The parameter u_o is obtained from the transcendental relation

$$\frac{V^2}{gh} u = \tanh(u)$$

and v_n is the solution of

$$\frac{V^2}{gh} v = \tan(v)$$

These functions are plotted in figures 7 and 8. As stated in reference 7, the function $\tanh(u)$ is nonperiodic, as shown in figure 7. The value of u_o can be determined from the intersection of the curve $\tanh(u)$ and a straight line drawn from the origin, having the angle β with the $+u$ axis such that $\tan \beta = \frac{V^2}{gh}$, since $\tan \beta = \frac{V^2}{gh} = \frac{\tanh(u_o)}{u_o}$. Hence, values for u_o exist if $\frac{V^2}{gh} \leq 1$; $u_o = 0$ for $\frac{V^2}{gh} = 1$. The function $\tan(v)$ of figure 8 is periodic and using the above procedure for determination of v_n the following solutions are obtained:

For $\frac{V^2}{gh} < 1$,

$$v_1, v_2, v_3, v_4 \cdots$$

and, for $\frac{V^2}{gh} > 1$,

$$v_o, v_1, v_2, v_3, v_4 \cdots$$

The infinite-series term of the Meyer equation seems to reduce to zero for values of $|x|$ near one-quarter wave length. The series term is important only in the vicinity of the hydrofoil, and after the first quarter wave length the theoretical surface is a sine wave that corresponds to the first term of the equation. The first part of the first term of the equation defines the amplitude of this sine wave which is dependent upon the circulation, velocity, depth of the hydrofoil submergence, depth of the channel, and the parameter u_o. As can be seen from the equation, the displacement varies directly with the circulation Γ and, therefore, with the lift coefficient. In this respect, the experimental data were in agreement with the two-dimensional theory. (See fig. 5.)

The second part of the first term defines the wave length and this part of the Meyer equation is identical with the usual equation for the wave length in shallow water. (See ref. 1.) The two-dimensional surface wave as calculated from the Meyer equation is shown in figure 5 for comparison with the experimental data.

At V^2/gh of 0.2, experiment and theory were in good agreement for the first half-wave length with the curves coincident from the trough to the free-water surface. The sine wave that was fitted to the data agreed with the Meyer wave except over the first quarter wave length behind the hydrofoil. This difference was due to the second term of the Meyer equation. At V^2/gh of 0.4, the maximum amplitudes were approximately the same but the length of the experimental profile was less than predicted by the theory. At V^2/gh of 0.6, both the amplitude and length of the experimental profile were less than the theoretical wave.

In the region investigated, comparison of the experimental profiles with the two-dimensional theory indicates that the surface wave can be predicted by two-dimensional theory from the trailing edge to the point of maximum upwash, but only at low subcritical speeds (V^2/gh of 0.2) and near the center line. Even near the center line where agreement with the two-dimensional theory might be expected, effects of finite aspect ratio apparently were large at V^2/gh of 0.4 and effects of finite aspect ratio and probably the channel depth were appreciable at V^2/gh of 0.6. Outboard of the center line, the surface pattern was complicated by the tip disturbances and no valid comparison with Meyer's two-dimensional theory was possible.

Downwash

Depth variation.- A plot of the variation of the angle of downwash with distance below the free-water surface at 0.1 semispan for V^2/gh of 0.2 is presented in figure 9 for five positions behind the hydrofoil and three angles of attack. As the distance below the surface increased, the angle of downwash decreased and appeared to approach the zero downwash or undisturbed condition asymptotically.

According to the theory for gravity waves, reference 1, the angles of downwash would be expected to decrease with distance below the free-water surface by the factor $e^{-\frac{2\pi d_c}{\lambda}}$, where d_c is the distance between orbit centers of the generating circles of the trochoidal wave. The angle of downwash at the surface was determined from the slope of the theoretical sine wave. By using the length of this sine wave the decrement with depth was calculated and is shown in figure 9 as the dashed line. In general,

the experimental and the calculated results were in good agreement for a distance aft of the hydrofoil of approximately 11 chords. At distances greater than 11 chords, the experimental data did not agree with the calculated values because of the disagreement between the experimental and theoretical surface waves at large distances behind the hydrofoil.

At values of V^2/gh greater than 0.2 and at other spanwise positions, the wave lengths and surface slopes did not agree with those given by two-dimensional theory and consequently the angles of downwash did not agree. Further analysis of the data indicated that the measured values, in general, varied exponentially with depth as would be expected for gravity waves.

Longitudinal variation.- The variation of the angle of downwash with distance behind the trailing edge of the hydrofoil at 0.1 semispan is presented in figures 10(a), 10(b), and 10(c) for values of V^2/gh of 0.2, 0.4, and 0.6, respectively. Following the procedure used with displacement of the water surface, the angle of downwash in degrees divided by the local lift coefficient is plotted against distance from the trailing edge. When divided by the local lift coefficient, the data for angles of attack of 2°, 4°, and 6° collapsed and the angles of downwash, therefore, varied directly with lift coefficient. The values of ϵ/c_l for the theoretical sine wave were calculated and are shown as the dashed line for the four depths below the surface.

At V^2/gh of 0.2, the experimental data were in good agreement with the calculated values at depths from 0.75c to 3.00c for the first half-wave length behind the trailing edge of the hydrofoil, that is, to the point of maximum upwash. Aft of this point, the experimental angles of downwash were not in agreement with the calculated values. This disagreement would be expected, however, because the slope of the experimental surface profile differed from that of the theoretical wave in this region.

At V^2/gh of 0.4 (fig. 10(b)) and 0.6 (fig. 10(c)), the values of the angles of downwash departed rapidly from the calculated values as the distance behind the hydrofoil was increased. In the region of upwash, the maximum experimental values were generally less than the calculated angles of upwash, and occurred at different locations behind the hydrofoil. This difference in location of the experimental and calculated maximums, which was particularly large at V^2/gh of 0.6, would be expected because the length of the experimental surface profiles differed from that of the theoretical waves. The data of figure 10 indicate, therefore, that the angles of downwash can be predicted by two-dimensional theory over the same range for which the theory accurately predicts the surface wave.

Spanwise variation.- The variations of the angle of downwash with distance from the plane of symmetry at 4° angle of attack are presented in figures 11(a), 11(b), and 11(c) for values of V^2/gh of 0.2, 0.4, and 0.6, respectively. Data are presented at four spanwise locations, at four depths below the free-water surface, and at several stations behind the trailing edge of the hydrofoil. The data have not been faired and the test points have simply been connected by straight lines.

The downwash pattern below the surface became complex as did the water surface. Near the surface, the spanwise variations in angle of flow were large and changed rapidly from downwash to upwash. The angles were particularly large at the 0.9-semispan position where the tip disturbance would be expected to influence the direction of flow. At depths greater than 2 chords, the angles of downwash and upwash were relatively small and did not vary greatly spanwise.

CONCLUSIONS

The results of the investigation of the surface and downwash patterns behind an aspect-ratio-10 hydrofoil led to the following conclusions:

1. The displacement of the free-water surface and the angles of downwash vary directly with lift coefficient as predicted by two-dimensional theory.

2. The angles of downwash vary exponentially with depth below the water surface as would be expected for gravity waves.

3. In the region investigated, the surface wave can be predicted by two-dimensional theory from the trailing edge to the point of maximum upwash, but only at low subcritical speeds and near the center line.

4. The angles of downwash can be predicted by two-dimensional theory over the same range for which the theory accurately predicts the surface wave.

5. Outboard of the center plane, the surface and downwash patterns are complicated by the tip disturbances and no valid comparison with two-dimensional theory is possible.

Langley Aeronautical Laboratory,
National Advisory Committee for Aeronautics,
Langley Field, Va.

[redacted]

REFERENCES

1. Lamb, Horace: Hydrodynamics. Reprint of sixth ed. (first American ed.), Dover Publications (New York), 1945, ch. IX, pp. 363-475.

2. Meyer, Rudolf X.: Two-Dimensional Vortex-Line Theory of a Hydrofoil Operating in Water of Finite Depth. Tech. Rep. HR-1, The Hydrofoil Corp., Nov.29, 1950.

3. Weinblum, Georg P.: Analysis of Wave Resistance. Rep. 710, David W. Taylor Model Basin, Navy Dept., Sept. 1950.

4. Wadlin, Kenneth L., Ramsen, John A., and McGehee, John R.: Tank Tests at Subcavitation Speeds of an Aspect-Ratio-10 Hydrofoil With a Single Strut. NACA RM L9K14a, 1950.

5. DeYoung, John: Theoretical Additional Span Loading Characteristics of Wings With Arbitrary Sweep, Aspect Ratio, and Taper Ratio. NACA TN 1491, 1947.

6. Wadlin, Kenneth L., Shuford, Charles L., Jr., and McGehee, John R.: A Theoretical and Experimental Investigation of the Lift and Drag Characteristics of a Hydrofoil at Subcritical and Supercritical Speeds. NACA RM L52D23a, 1952.

7. Vavra, M. H.: Wave Drag of Submerged Foils in Shallow Water. Tech. Memo. No. HM-3 (Contract Nonr - 13601), The Hydrofoil Corp., Nov. 19, 1950.

TABLE I

LIFT COEFFICIENTS

$\frac{V^2}{gh}$	α, deg	C_L	c_l at 0.1b
0.2	2	0.255	0.292
	4	.375	.429
	6	.475	.544
.4	2	.307	.352
	4	.435	.498
	6	.540	.618
.6	2	.330	.378
	4	.460	.527
	6	.570	.653

NACA

[redacted]

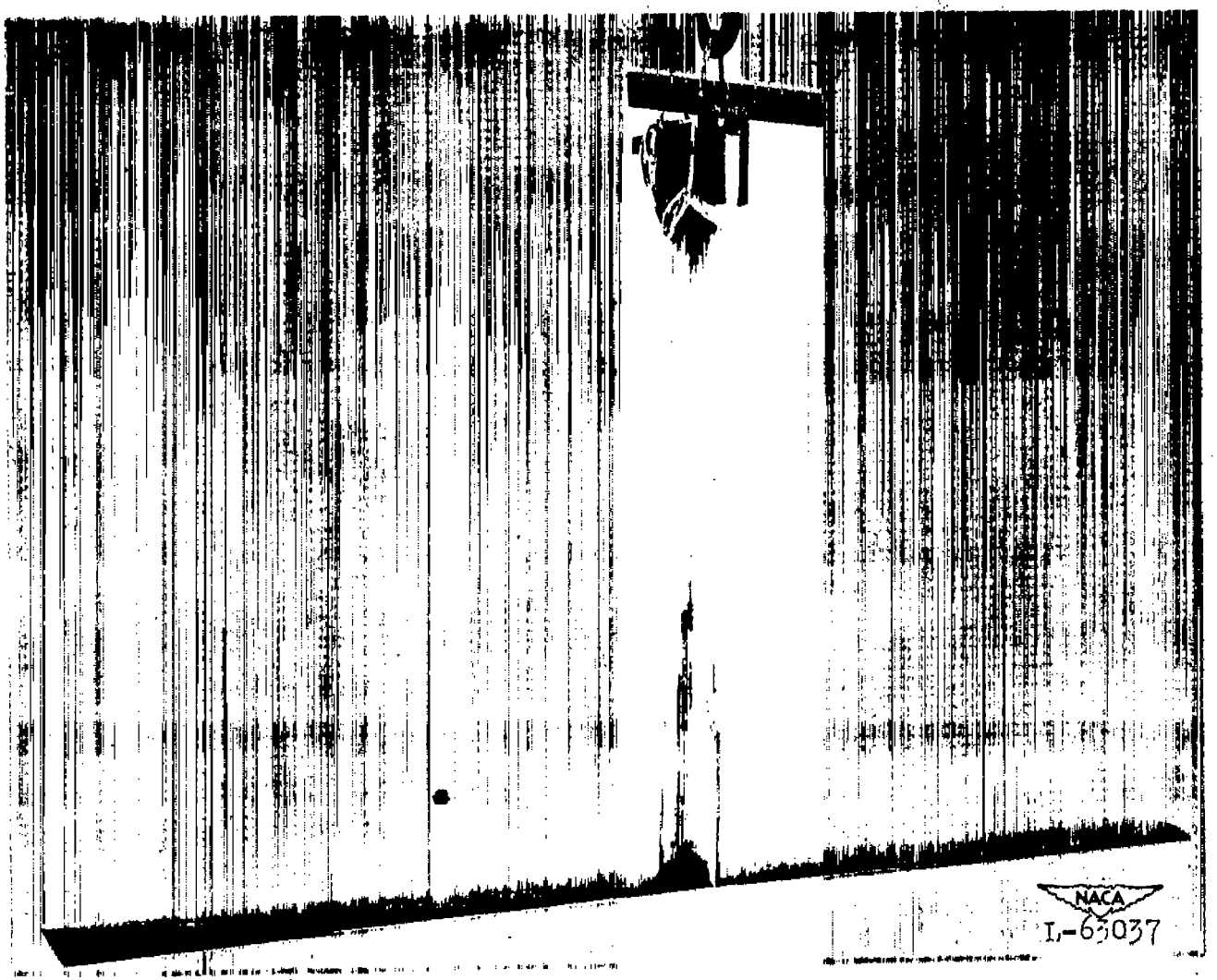

Figure 1.- Hydrofoil and strut.

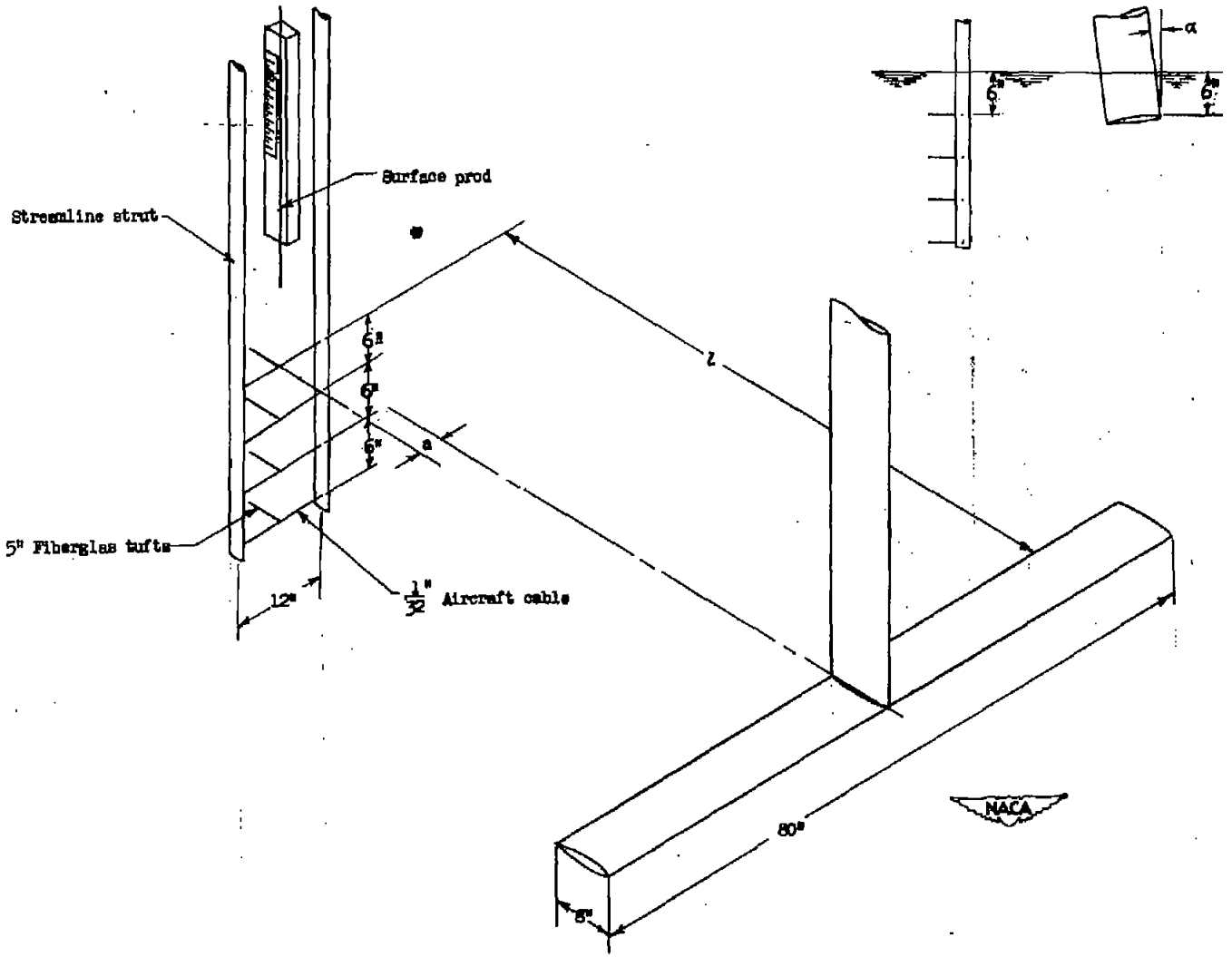

Figure 2.- Setup for investigation of downwash behind hydrofoil.

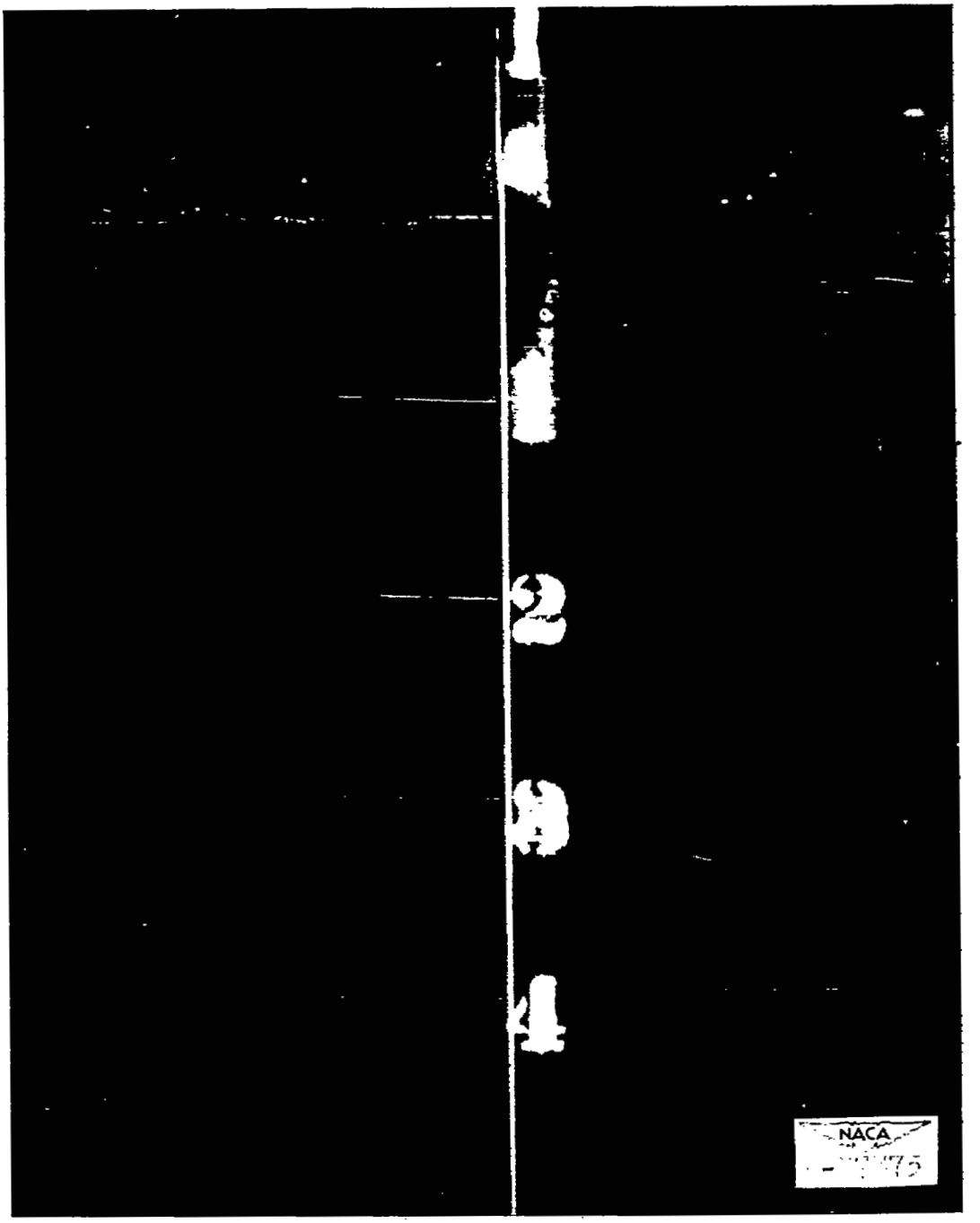

Figure 3.- Typical underwater photograph of tufts.

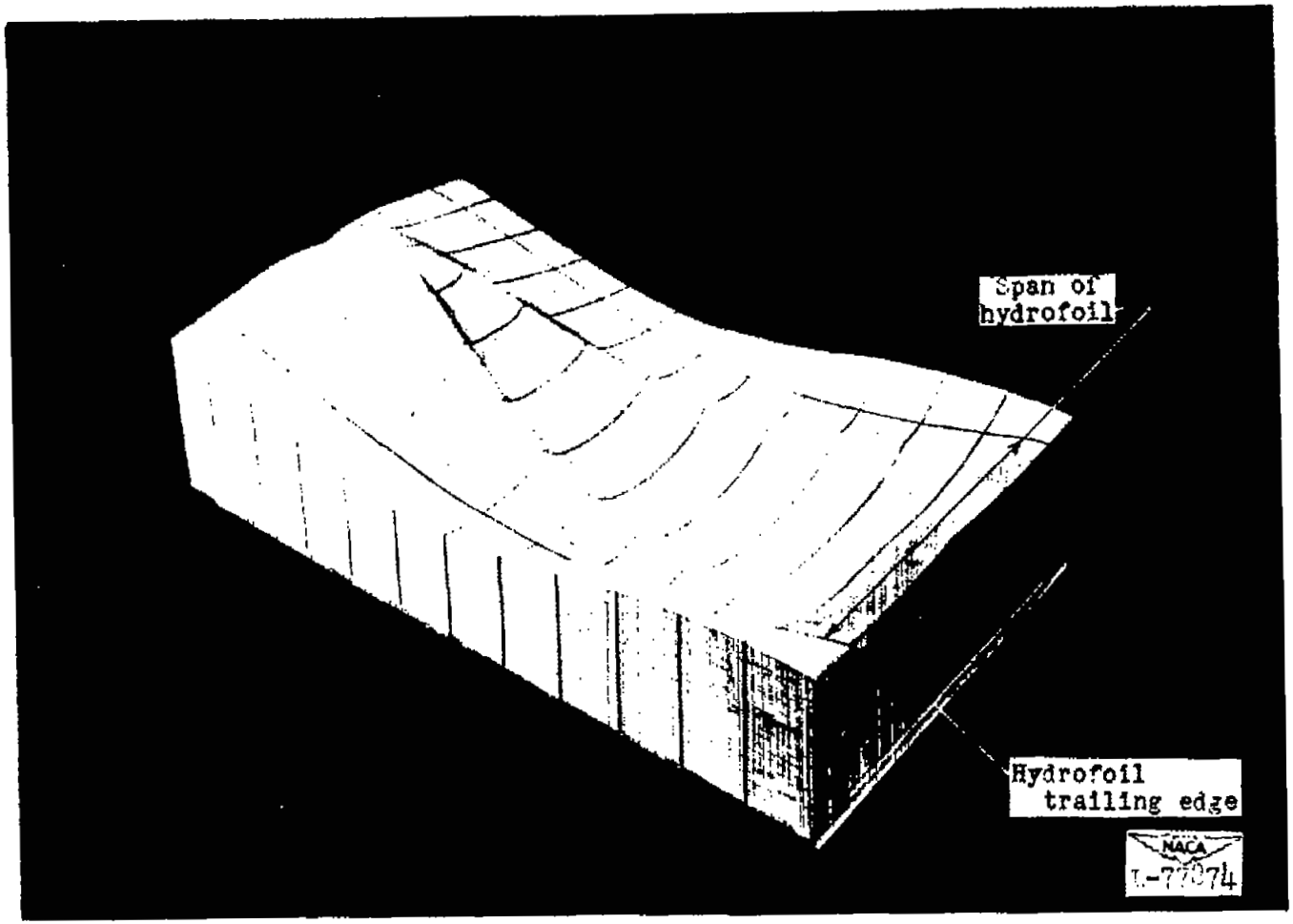

Figure 4.- Photograph of model of typical surface pattern. Vertical scale enlarged five times; $\frac{V^2}{gh} = 0.4$, $\alpha = 4^\circ$.

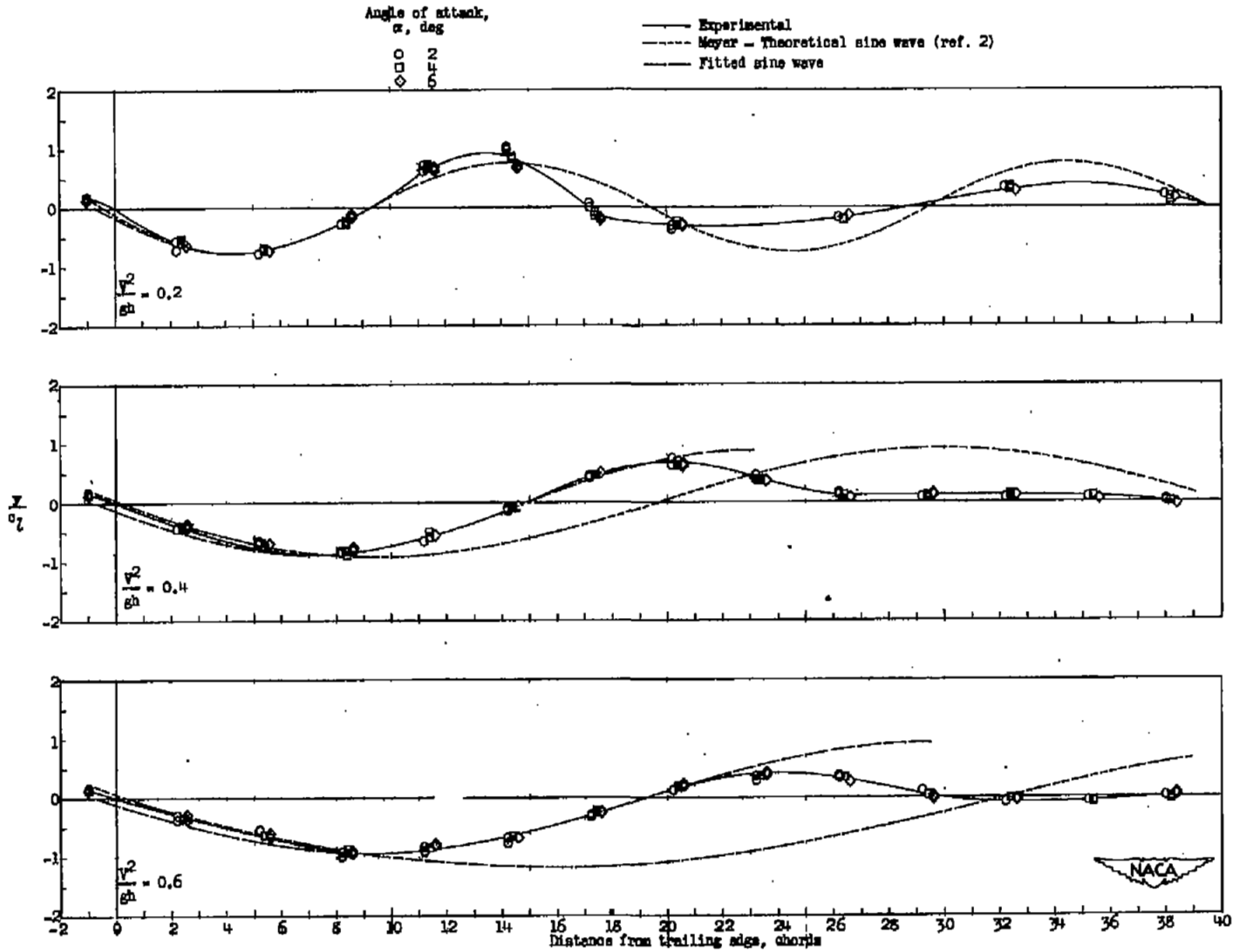

Figure 5.- Longitudinal surface profiles behind hydrofoil at 0.1 semispan.

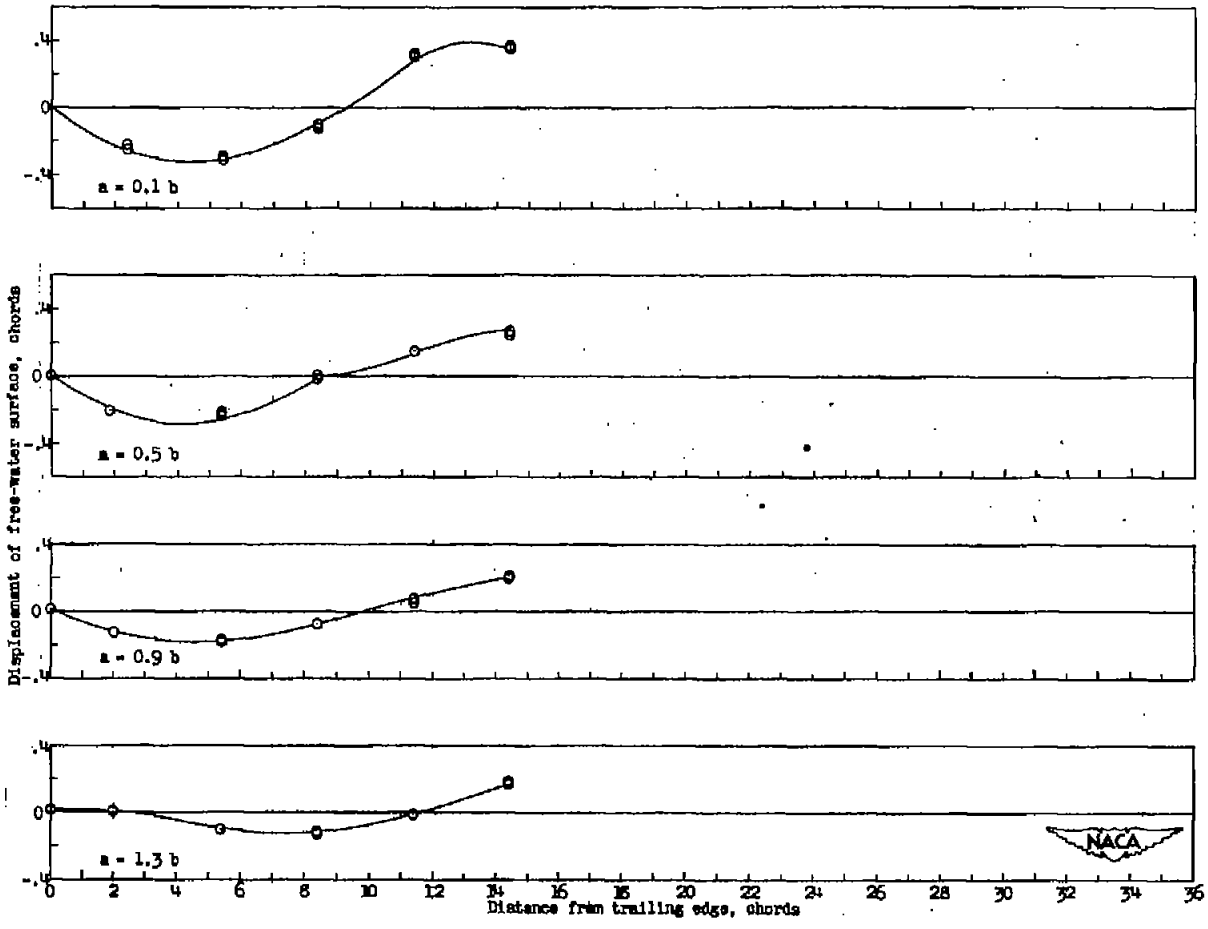

(a) $\frac{V^2}{gh} = 0.2$.

Figure 6.- Longitudinal surface profiles behind hydrofoil at 4° angle of attack for four spanwise positions.

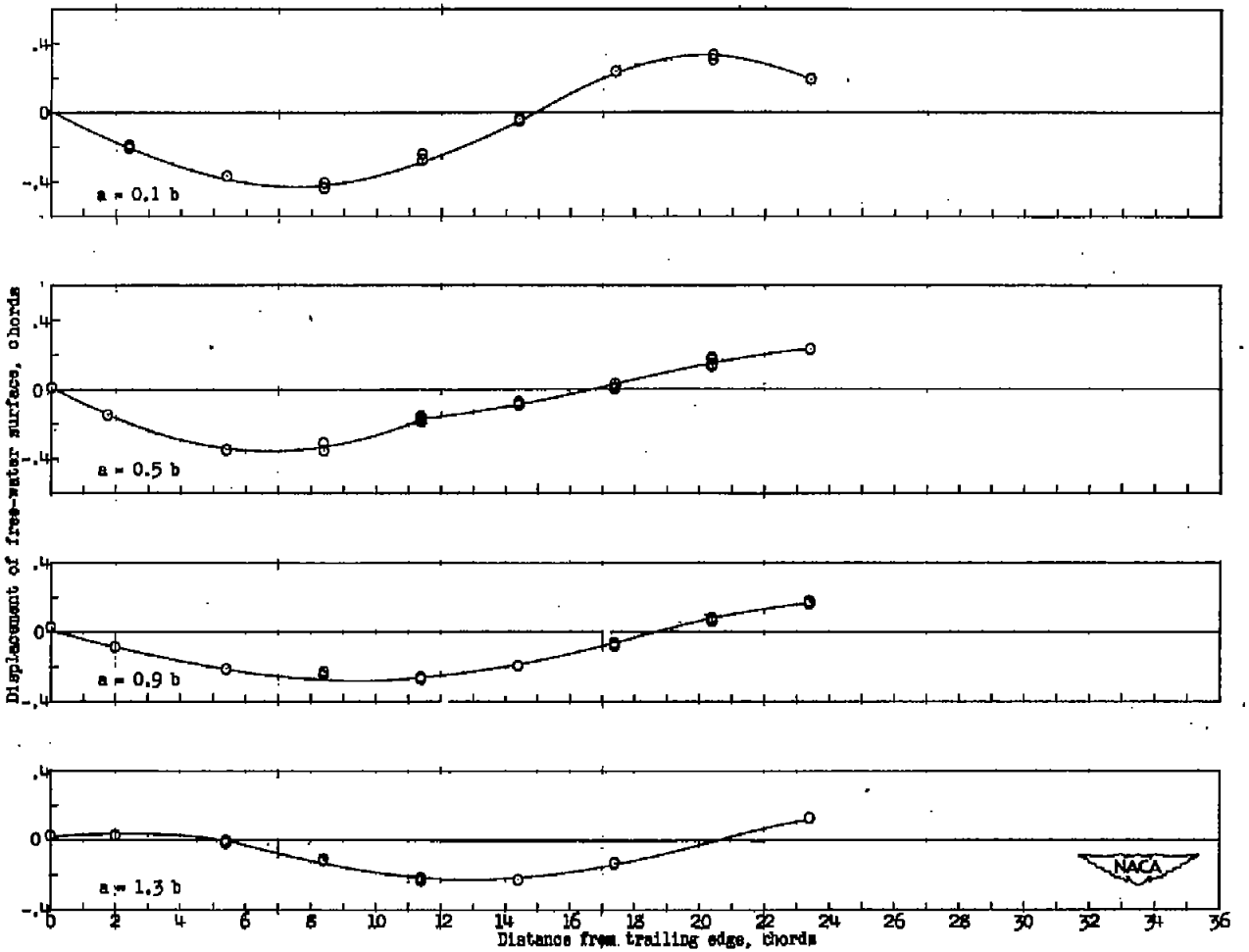

(b) $\frac{V^2}{gh} = 0.4$.

Figure 6.- Continued.

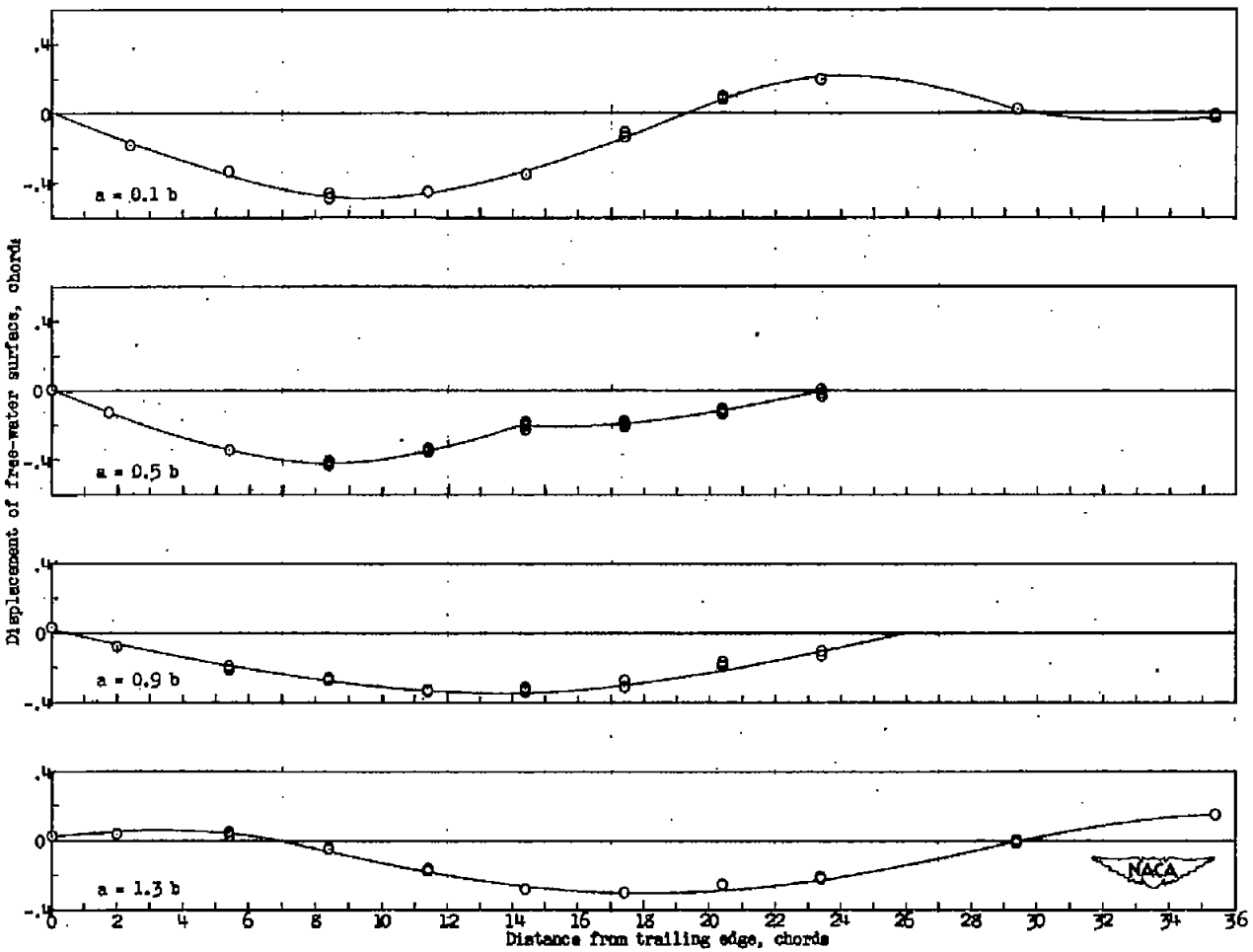

(c) $\frac{V^2}{gh} = 0.6$.

Figure 6.- Concluded.

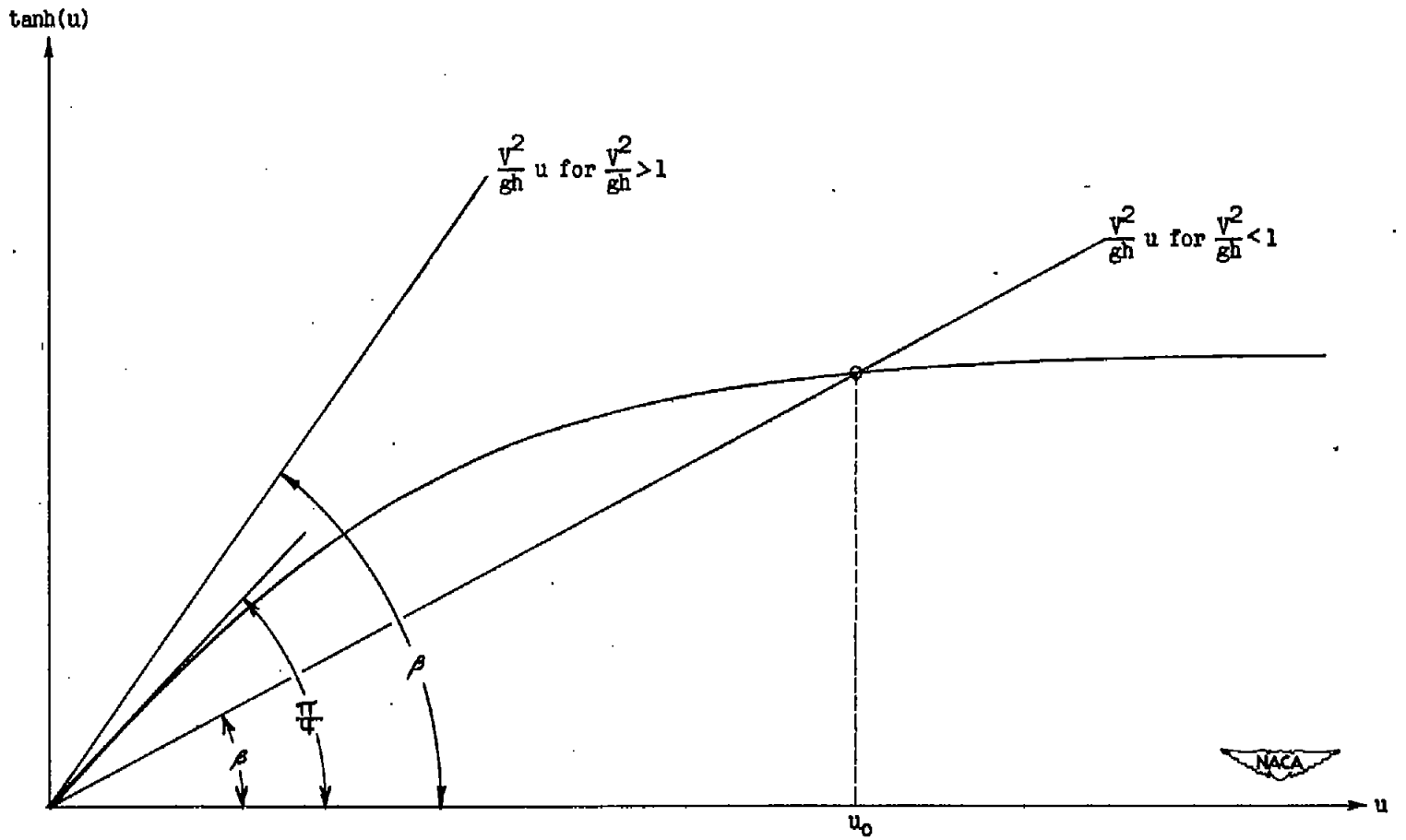

Figure 7.- Variation of tanh(u) with u.

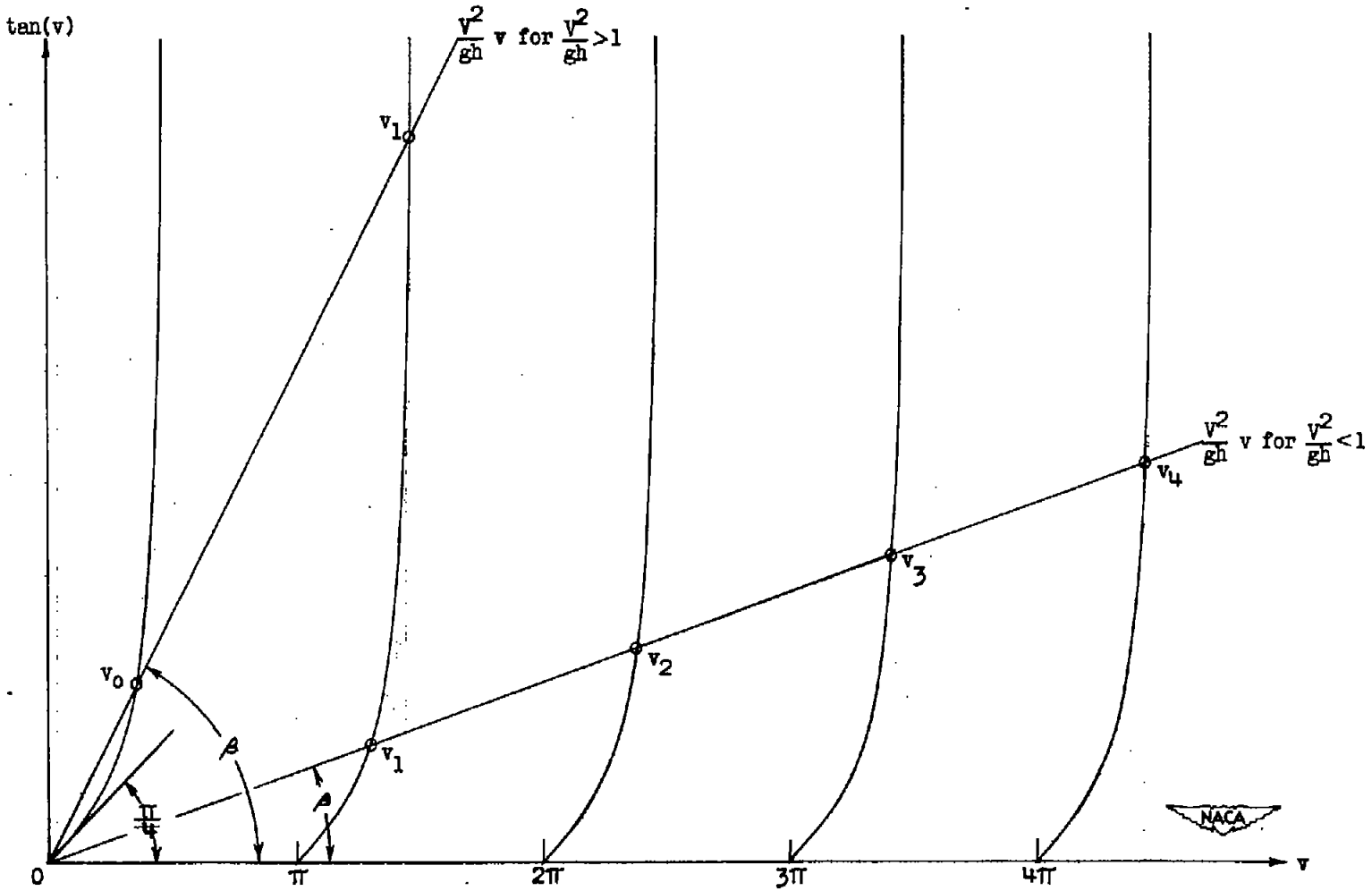

Figure 8.- Variation of tan(v) with v.

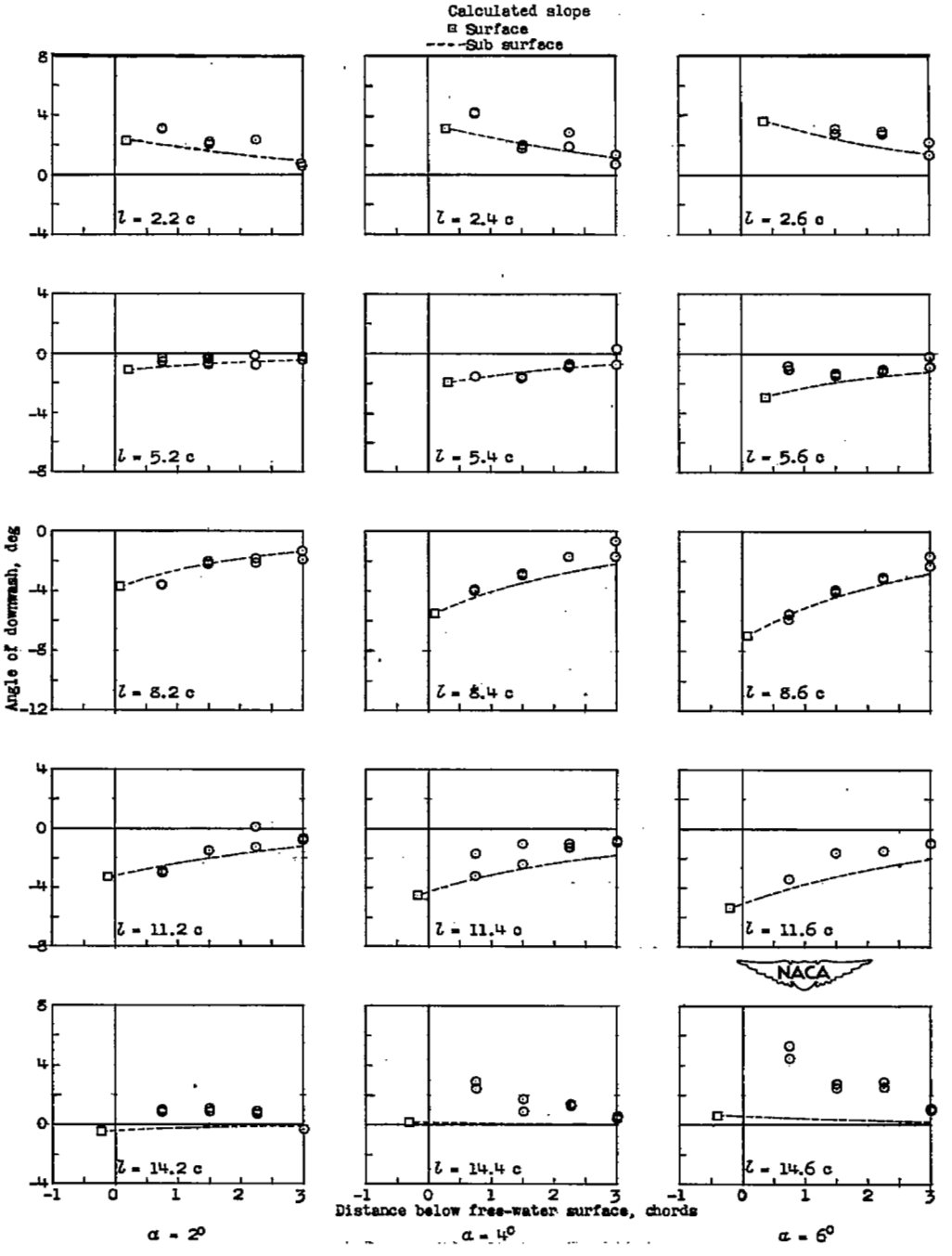

Figure 9.- Variation of angle of downwash with distance below free-water surface at 0.1 semispan. Hydrofoil at three angles of attack; $\frac{V^2}{gh} = 0.2$.

[redacted]

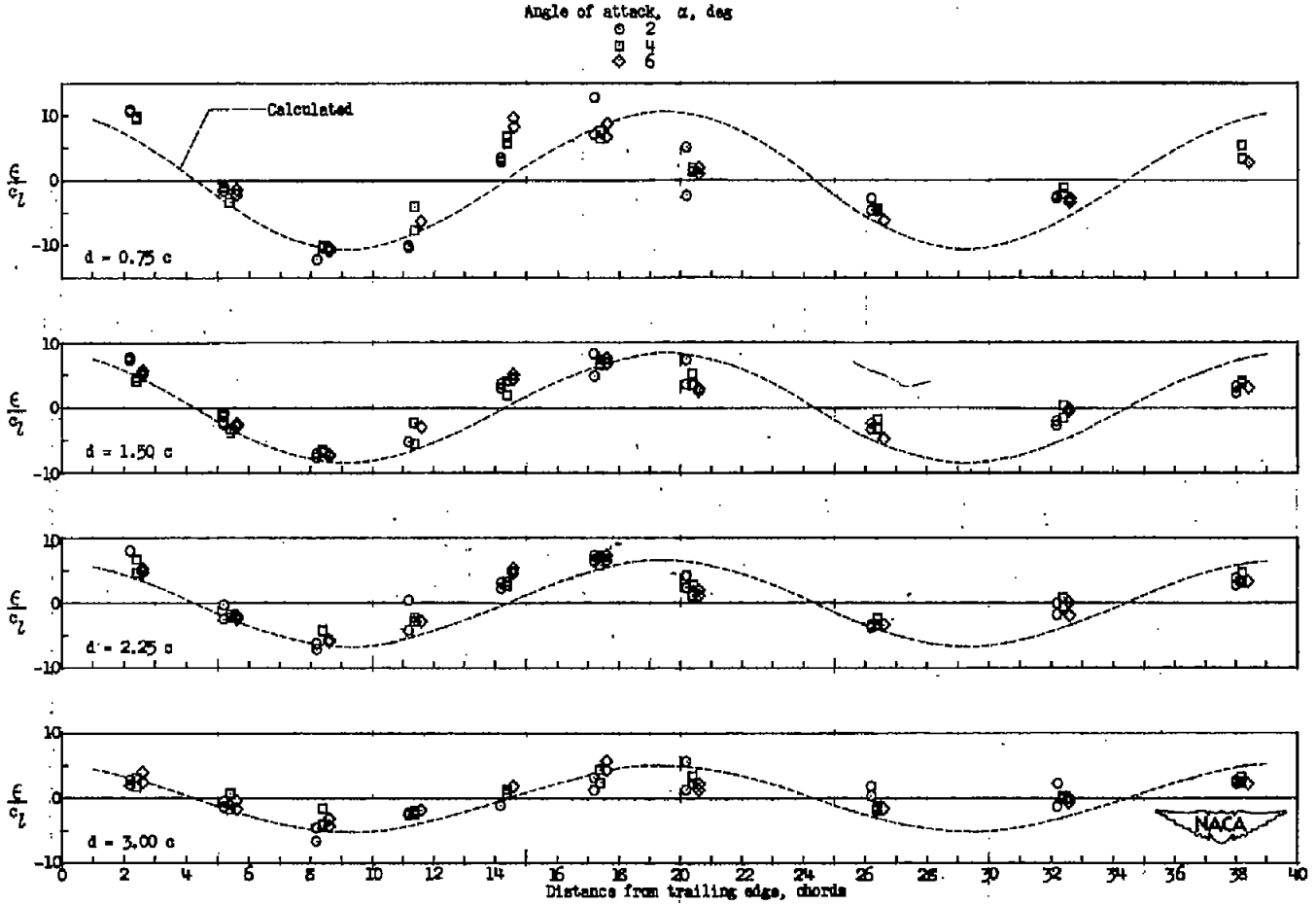

(a) $\frac{V^2}{gh} = 0.2$.

Figure 10.- Variation of downwash with distance behind trailing edge of hydrofoil at 0.1 semispan.

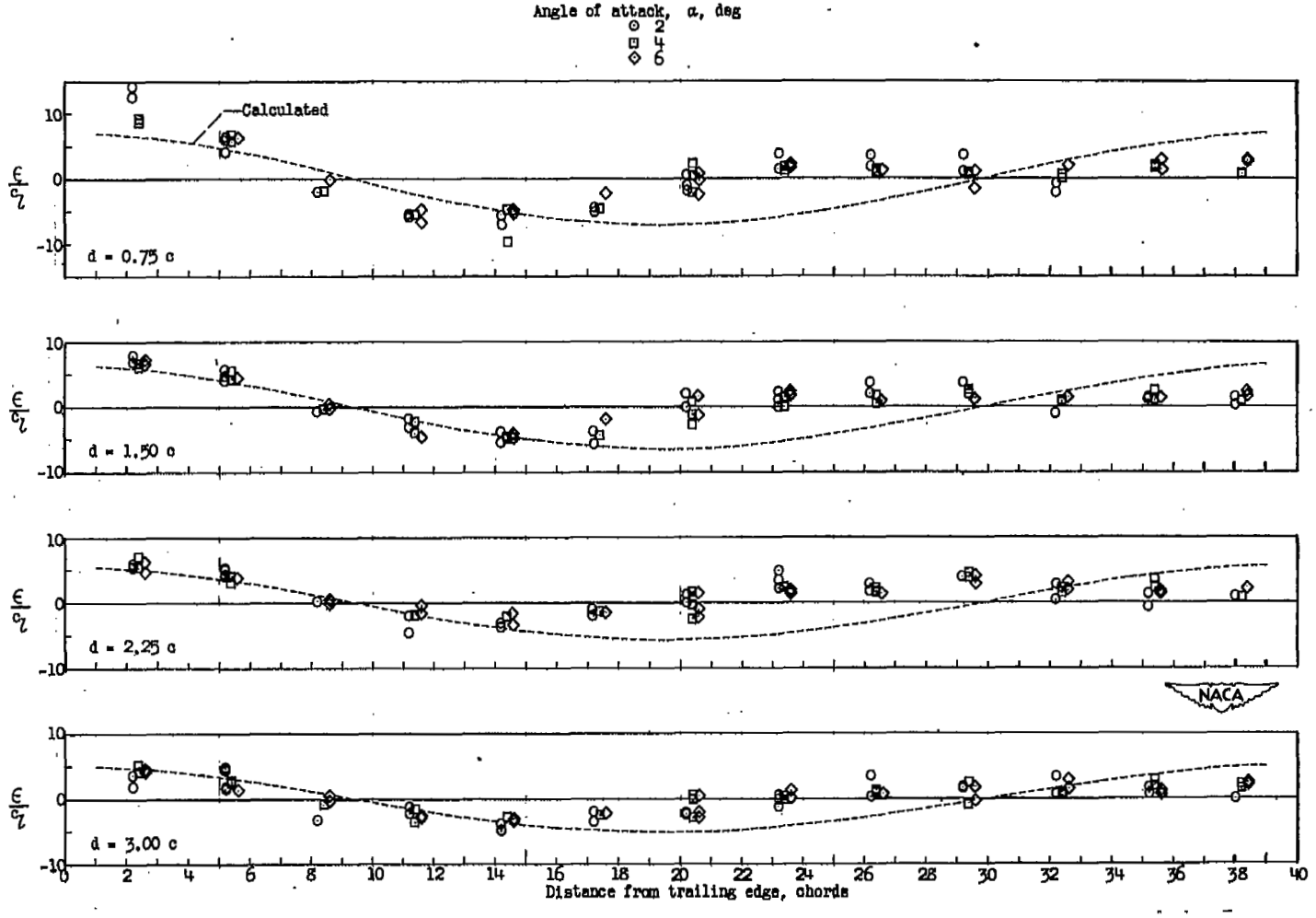

(b) $\frac{V^2}{gh} = 0.4$.

Figure 10.- Continued.

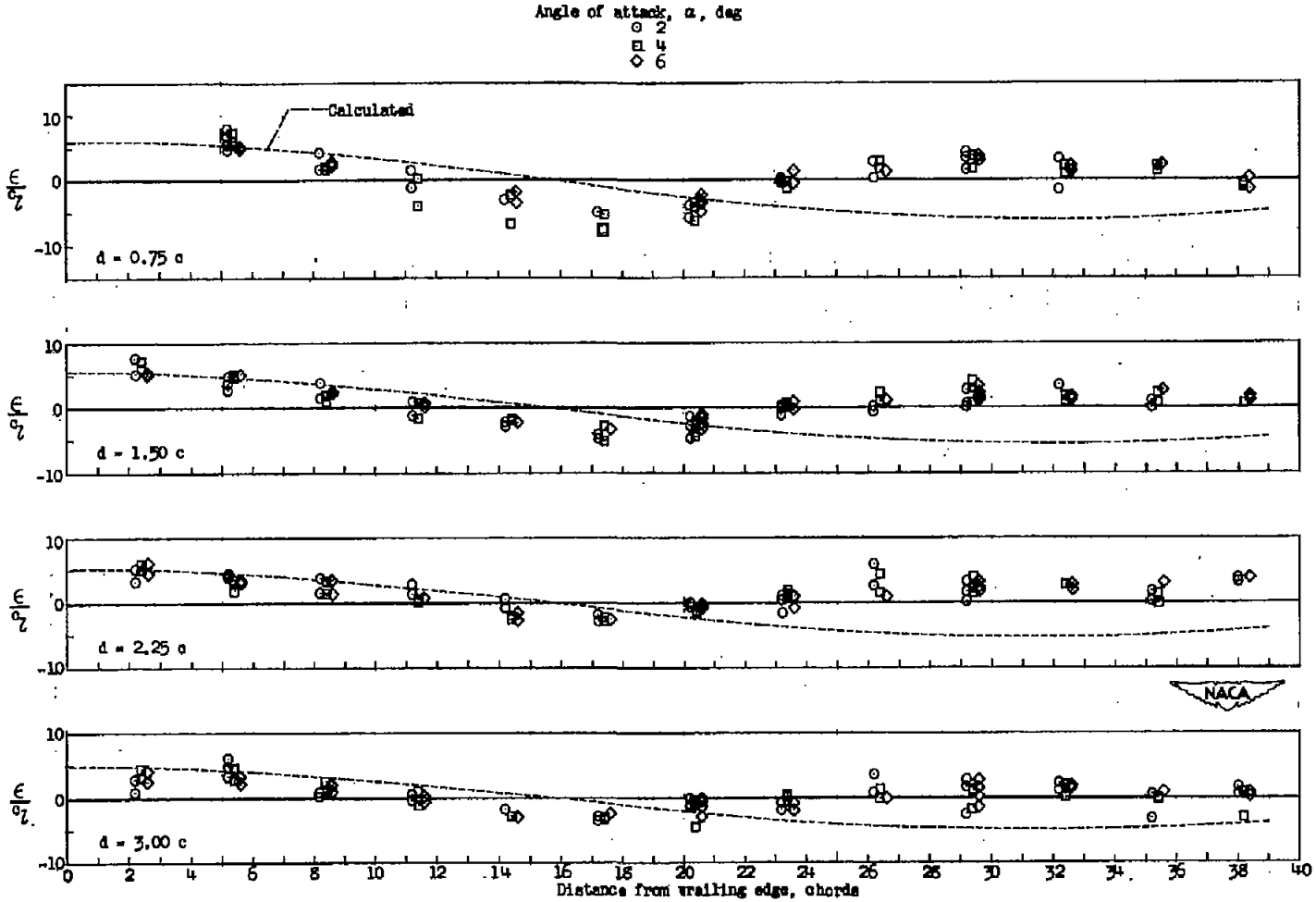

(c) $\frac{V^2}{gh} = 0.6$.

Figure 10.- Concluded.

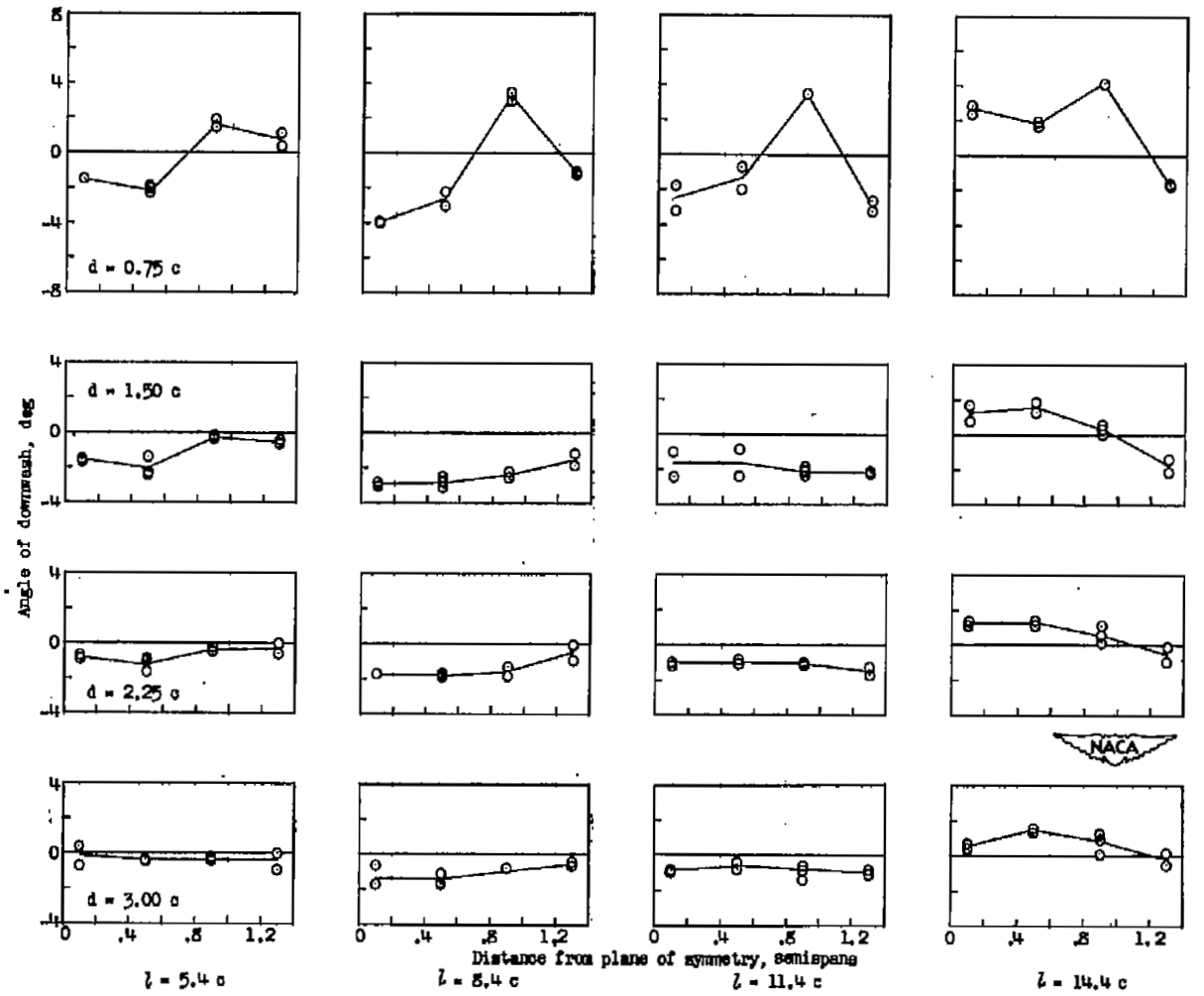

(a) $\frac{V^2}{gh} = 0.2$.

Figure 11.- Variation of angle of downwash with distance from plane of symmetry for four depths below free-water surface. $\alpha = 4^\circ$.

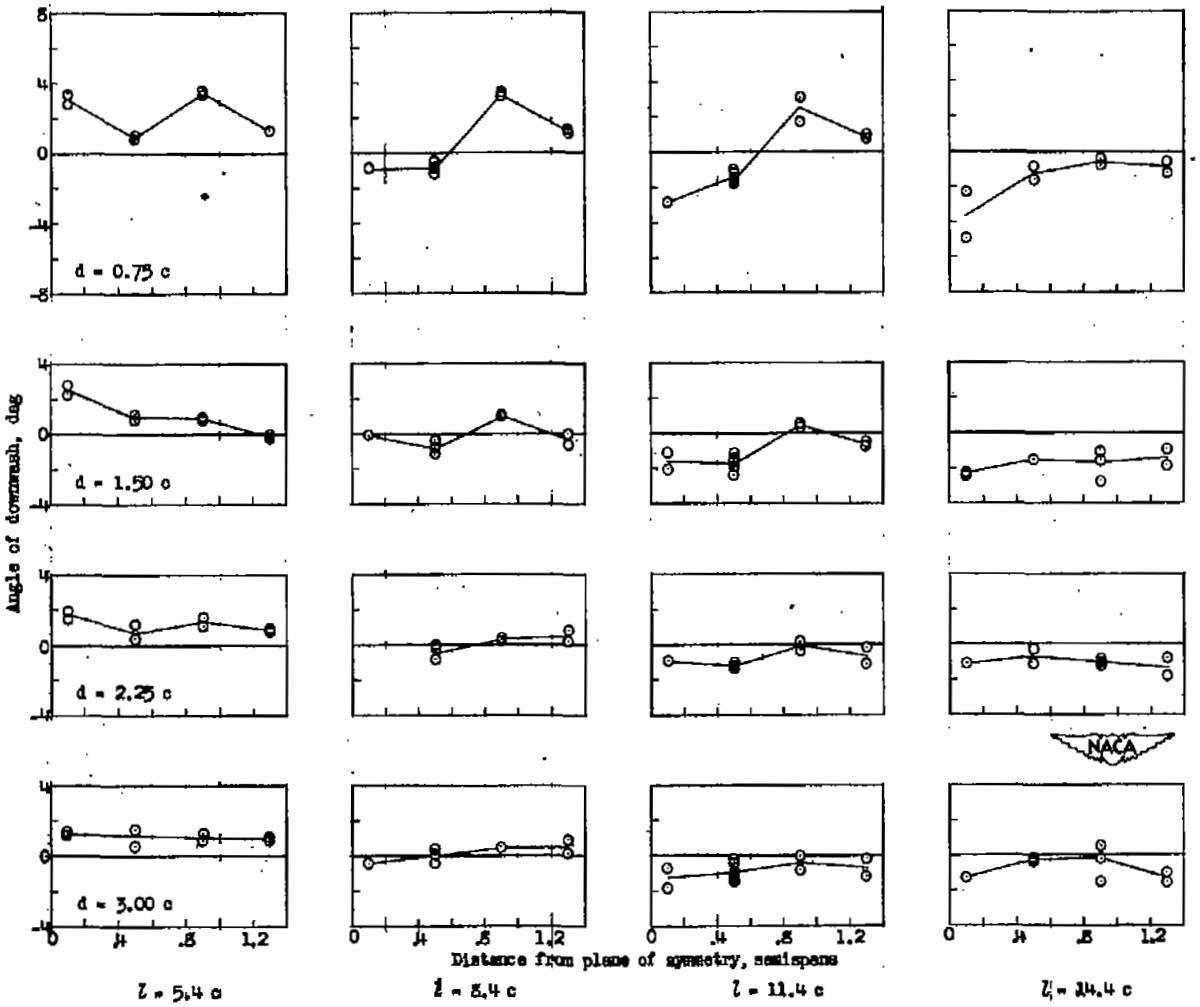

(b) $\frac{V^2}{gh} = 0.4$.

Figure 11.- Continued.

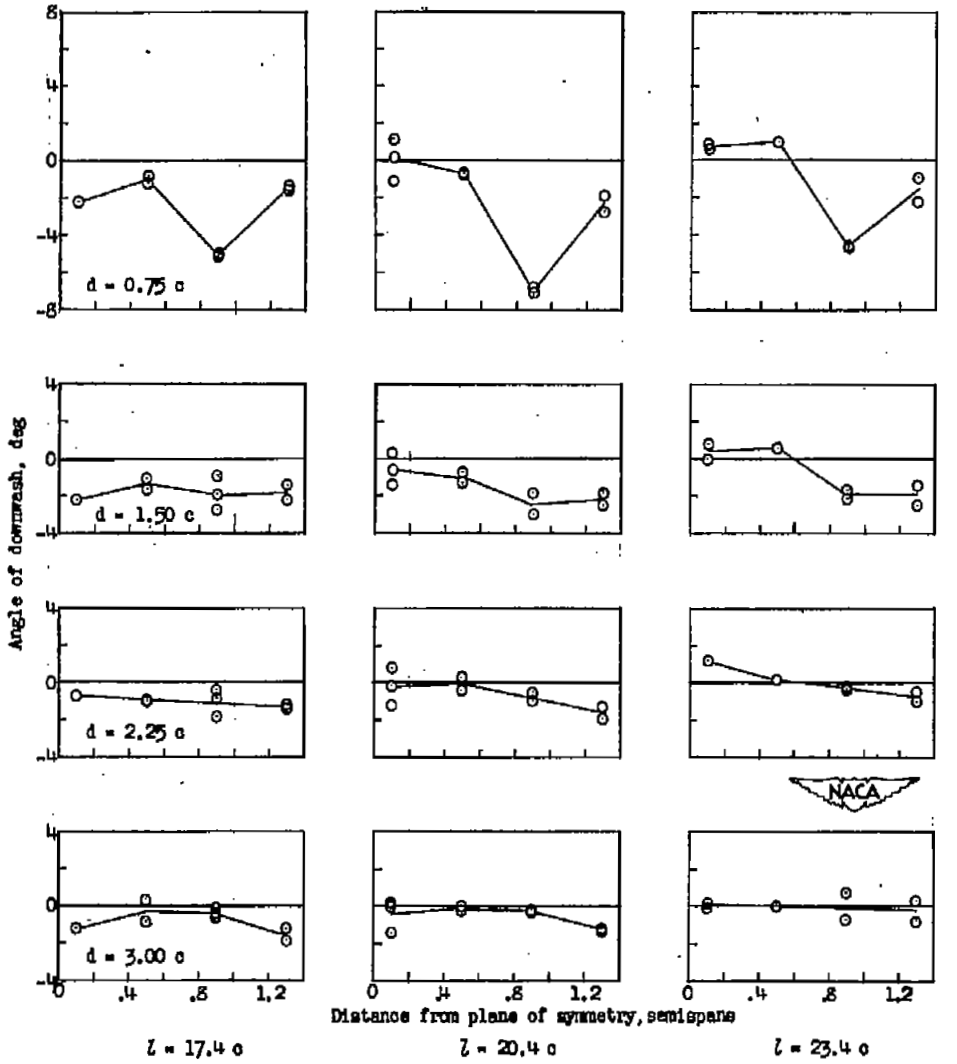

(b) Concluded.

Figure 11.- Continued.

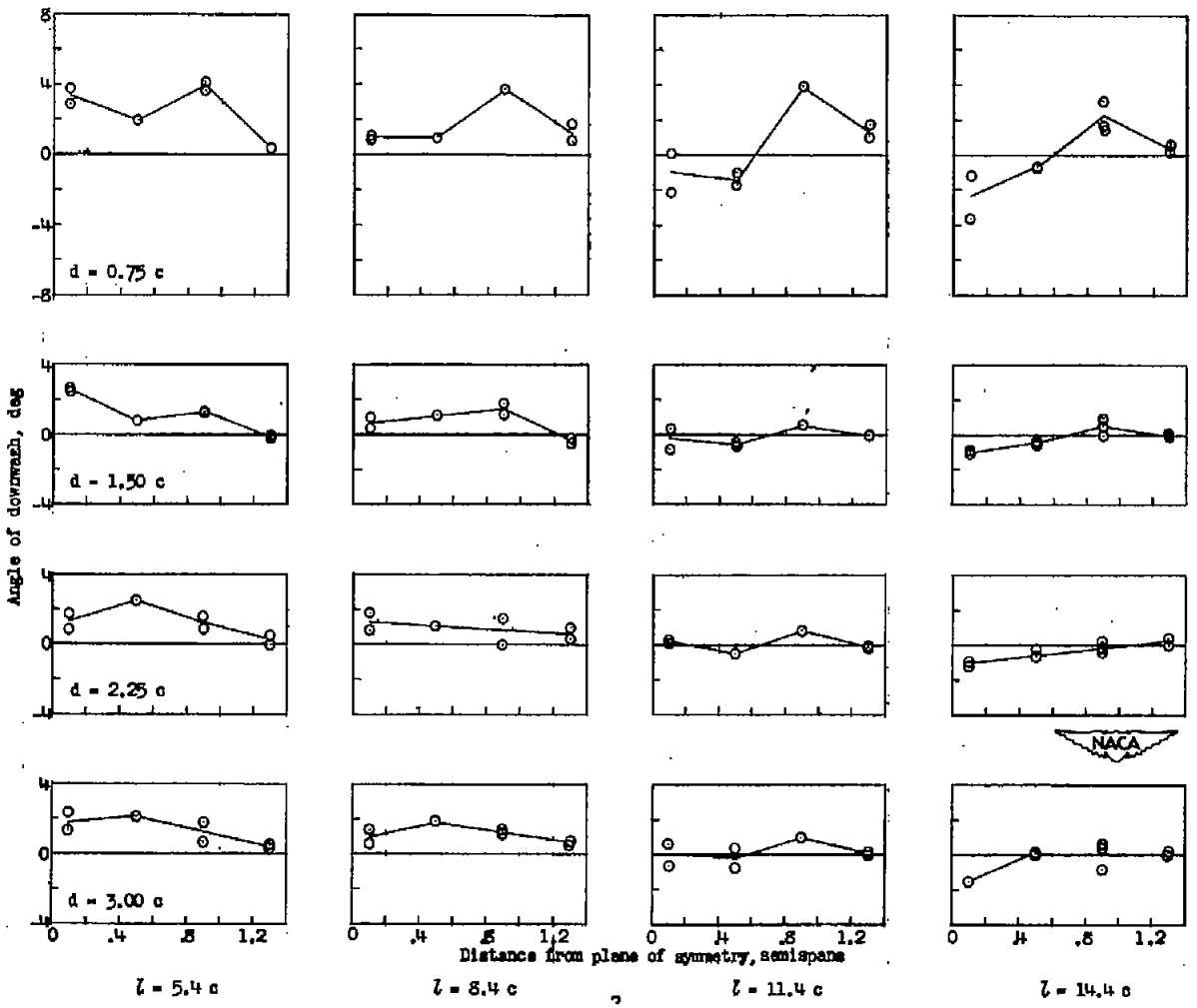

(c) $\frac{V^2}{gh} = 0.6$.

Figure 11.- Continued.

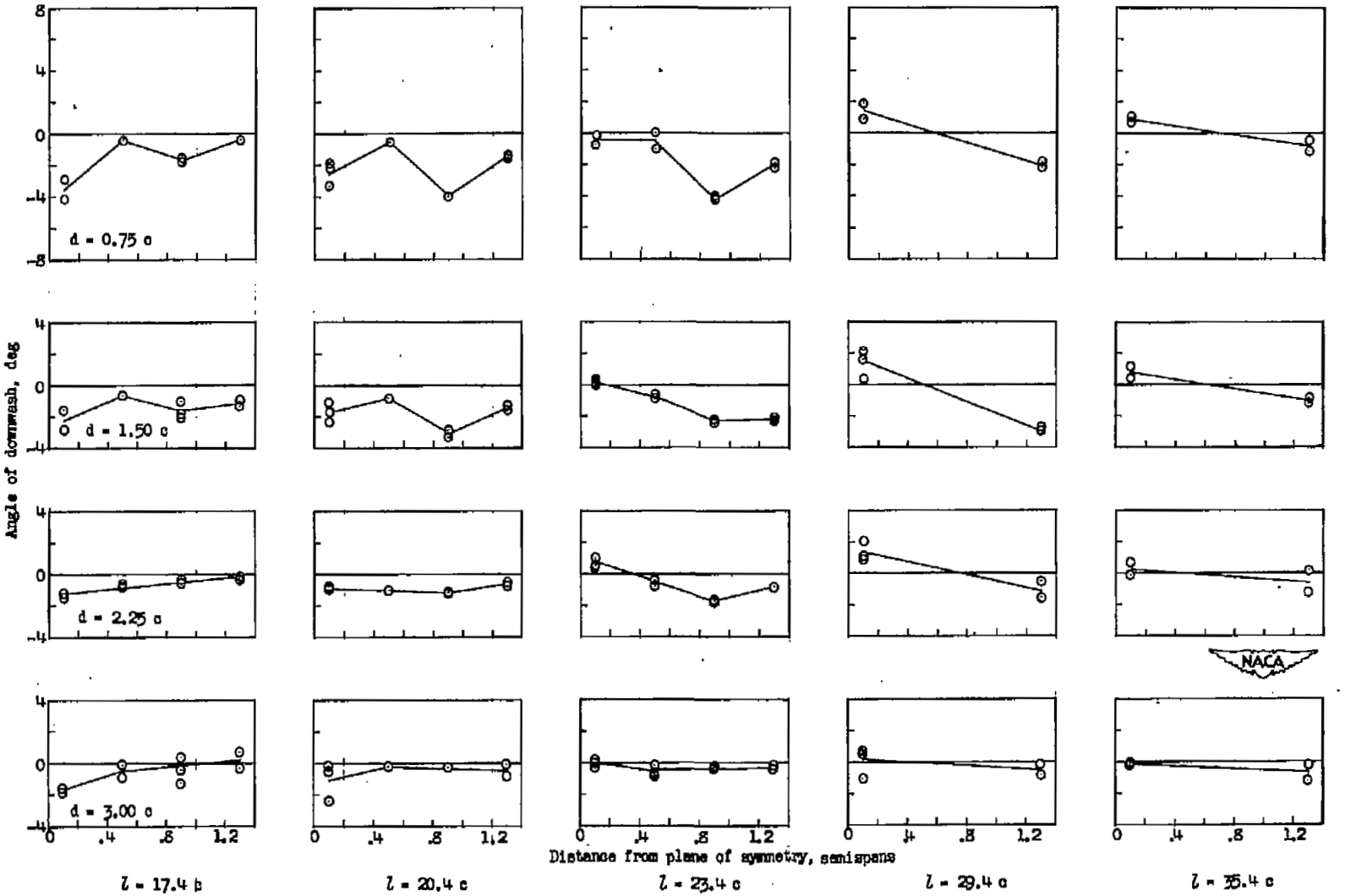

(c) Concluded.

Figure 11.- Concluded.